

# MSEMG: Surface Electromyography Denoising with a Mamba-based Efficient Network

Yu-Tung Liu<sup>\*§</sup>, Kuan-Chen Wang<sup>†§</sup>, Rong Chao<sup>§¶</sup>, Sabato Marco Siniscalchi<sup>‡</sup>, Ping-Cheng Yeh<sup>†</sup>, and Yu Tsao<sup>§</sup>

<sup>\*</sup>Department of Electronics and Electrical Engineering, National Yang Ming Chiao Tung University, Taiwan

<sup>†</sup>Graduate Institute of Communication Engineering, National Taiwan University, Taiwan

<sup>¶</sup>Department of Computer Science and Information Engineering, National Taiwan University, Taiwan

<sup>‡</sup>University of Palermo, Italy <sup>§</sup>Research Center for Information Technology Innovation, Academic Sinica, Taiwan

Email: tonyliu.ee09@nycu.edu.tw, d12942016@ntu.edu.tw, roychao@cmlab.csie.ntu.edu.tw

sabatomarco.siniscalchi@unipa.it, pcyeh@ntu.edu.tw, yu.tsao@citi.sinica.edu.tw

**Abstract**—Surface electromyography (sEMG) recordings can be contaminated by electrocardiogram (ECG) signals when the monitored muscle is closed to the heart. Traditional signal-processing-based approaches, such as high-pass filtering and template subtraction, have been used to remove ECG interference but are often limited in their effectiveness. Recently, neural-network-based methods have shown greater promise for sEMG denoising, but they still struggle to balance both efficiency and effectiveness. In this study, we introduce MSEMG, a novel system that integrates the Mamba State Space Model with a convolutional neural network to serve as a lightweight sEMG denoising model. We evaluated MSEMG using sEMG data from the Non-Invasive Adaptive Prosthetics database and ECG signals from the MIT-BIH Normal Sinus Rhythm Database. The results show that MSEMG outperforms existing methods, generating higher-quality sEMG signals with fewer parameters. The source code for MSEMG is available at <https://github.com/tonyliu0910/MSEMG>.

**Index Terms**—Surface electromyography, State space model, ECG interference removal, Deep neural network

## I. INTRODUCTION

Surface electromyography (sEMG) captures electrical motor nerve signals and converts them into digital recordings. sEMG signals are measured by sensors noninvasively, providing rich clinical insights into muscular activities. sEMG has hitherto been applied in a variety of applications, including neuromuscular system investigation [1], rehabilitation [2], stress monitoring [3], assessment of neuromuscular or respiratory disorders [4], [5], prosthesis control [6], and gesture recognition in virtual reality (VR) [7], [8]. However, sEMG signals can be contaminated by electrocardiography (ECG) signals when sensors are placed near the thorax. This interference lowers the quality and fidelity of sEMG recordings, which can impact clinical outcomes and human-computer interactions.

sEMG and ECG signals share the frequency band of 0 to 100 Hz [9], making it complicated to eliminate ECG artifacts from sEMG. Some conventional signal-processing-based methods, such as high-pass filters (HP) and template subtraction (TS) [10], [11], struggle to extract clean sEMG signals, especially when dealing with low signal-to-noise ratios (SNRs). Given these challenges, neural networks (NNs) have been introduced into sEMG enhancement techniques due to their powerful nonlinear mapping capability and data-driven

characteristics [12], [13]. [12] proposed a fully convolutional network (FCN), a discriminative model that outperformed traditional methods (HP and TS) in ECG artifact removal. [13] introduced a score-based diffusion model, a generative approach that achieved superior results compared to earlier techniques. However, diffusion models require high computational costs during inference, limiting their use in real-time or resource-constrained sEMG applications. This necessitates an efficient and high-performing sEMG denoising method.

The Mamba state space model (SSM) [14] is a prominent recurrent neural network (RNN) designed to effectively capture temporal information from long sequences with linear time complexity. This low computational cost distinguishes Mamba from Transformer [15], which also excels at handling global dependencies but requires more expensive quadratic time complexity. Due to its efficiency, Mamba has been applied to various domains, such as large language models [16] and signal enhancement [17]. However, its potential for sEMG denoising has not yet been explored, as previous methods primarily rely on Convolutional Neural Networks (CNNs).

In this study, we introduce MSEMG, a lightweight Mamba-inherited CNN designed to efficiently generate high-quality sEMG signals. By integrating Mamba with CNNs, MSEMG overcomes the limited receptive fields of convolutional layers and can capture both local and long-range dependencies. Experimental results demonstrate that MSEMG outperforms previous sEMG denoising techniques across several evaluation metrics. Furthermore, MSEMG adopts fewer parameters than the previous state-of-the-art sEMG denoising method. These findings suggest that MSEMG is a promising solution for providing high-quality signals for miscellaneous sEMG applications. To the best of our knowledge, this is the first study exploring Mamba’s application to sEMG processing.

The remainder of this paper is organized as follows. Section 2 reviews related works. Section 3 introduces the proposed approach. Section 4 presents the experimental setup and results. Finally, Section 5 concludes the paper and discusses future works.

## II. RELATED WORK

### A. ECG interference removal methods

Traditional methods like HP and TS [10], [11] have used classical signal-processing techniques to remove ECG artifacts from sEMG signals. However, these methods have limitations in achieving high-quality sEMG recordings. HP removes the frequency band associated with ECG interference and eliminates the low-frequency components of the sEMG. TS, on the other hand, operates in the time domain to handle ECG interference by extracting ECG templates through filtering or waveform averaging [10], [18]. However, TS may be less effective in real-world applications as it assumes the sEMG signals follow a zero-mean Gaussian distribution. This study implements both HP and TS methods for comparison in our experiments.

NN-based techniques have shown significant improvements in sEMG denoising. Wang et al. [12] introduced a fully convolutional network (FCN) as a denoising autoencoder to remove ECG artifacts from sEMG signals. The FCN consists of two main components: an encoder to extract features and a decoder to translate the latent representation back into the signal. This approach has yielded impressive results across various research areas, and the FCN has proven more powerful than traditional methods. However, it still struggles with some signal distortion.

To address these issues, SDEMG was introduced [13], applying the generative model to the problem of sEMG denoising. Diffusion models, known for generating high-quality and high-fidelity outputs, were used to identify noise during the diffusion process and remove ECG interference during sampling. While SDEMG is highly effective, the repeated inference steps lead to high computational costs, making it impractical for resource-limited sEMG applications.

### B. Mamba State Space Model

The Mamba State Space Model is a cutting-edge NN architecture designed for sequence modeling, particularly excelling in handling long sequences [14]. Mamba addresses some of the limitations of traditional Transformer models, especially in terms of computational efficiency and performance on various data modalities like language [16], audio [17], [19], and genomics [20], [21]. Though state space models exhibited limited performance previously, with the selective state space mechanism, Mamba could perform content-based reasoning, allowing it to propagate or neglect information based on the current token selectively. Moreover, Mamba offers linear scaling in sequence length and achieves faster inference, with up to 5 times higher throughput than Transformers. As a result, Mamba has shown state-of-the-art performance across several modalities, outperforming Transformers of the same size and matching those twice its size in both pretraining and downstream evaluation. Initially, the Mamba-3B model excels in language tasks, outperforming comparable Transformer models.

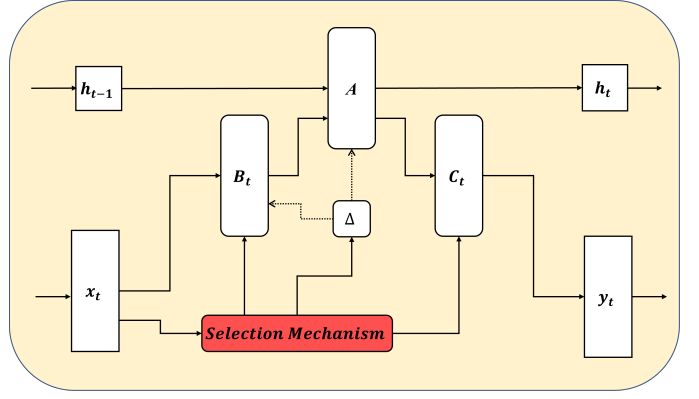


Fig. 1. The Selective State Space Model.

## III. THE PROPOSED METHOD

In this section, we introduce the Mamba model and the selection mechanism as a key proportion of this novel integration of CNN and the state space model. The implementation detail of the NN in this work will be further elaborated.

### A. Selective state space model

The Mamba SSM introduced a selective scan mechanism to perform sequence mapping from input  $x(t) \in \mathbb{R}$  to  $y(t) \in \mathbb{R}$  adaptively. There are some key elements in the SSM: a trainable parameter  $\Delta$ , a state transition matrix  $A \in \mathbb{R}^{H \times H}$ , an input projection matrix  $B \in \mathbb{R}^{H \times 1}$ , an output projection matrix  $C \in \mathbb{R}^{1 \times H}$ , and a hidden state  $h \in \mathbb{R}^H$ . Note that  $H$  indicates the dimension of the hidden state. Empirically, the dimension of the hidden state is determined by the complexity of the problem. The state transition process could be described by equation (1) and the output projection by equation (2).

$$h'(t) = Ah(t) + Bx(t) \quad (1)$$

$$y(t) = Ch(t) \quad (2)$$

While the equations above describe state transitions in continuous-time signals, it is important to note that discrete-time signals dominate actual experiments and downstream applications.  $\bar{A}$  and  $\bar{B}$  in equations (3) and (4) are the discretized matrices approximated by zero-order hold.

$$h_t = \bar{A}h_{t-1} + \bar{B}x_t \quad (3)$$

$$y_t = Ch_t \quad (4)$$

Learnable parameter  $\Delta$  adjusts the balance between the hidden state and the current input:

$$\bar{A} = \exp(\Delta A) \quad (5)$$

$$\bar{B} = (\Delta A)^{-1}(\exp(\Delta A) - I) \cdot \Delta B \quad (6)$$

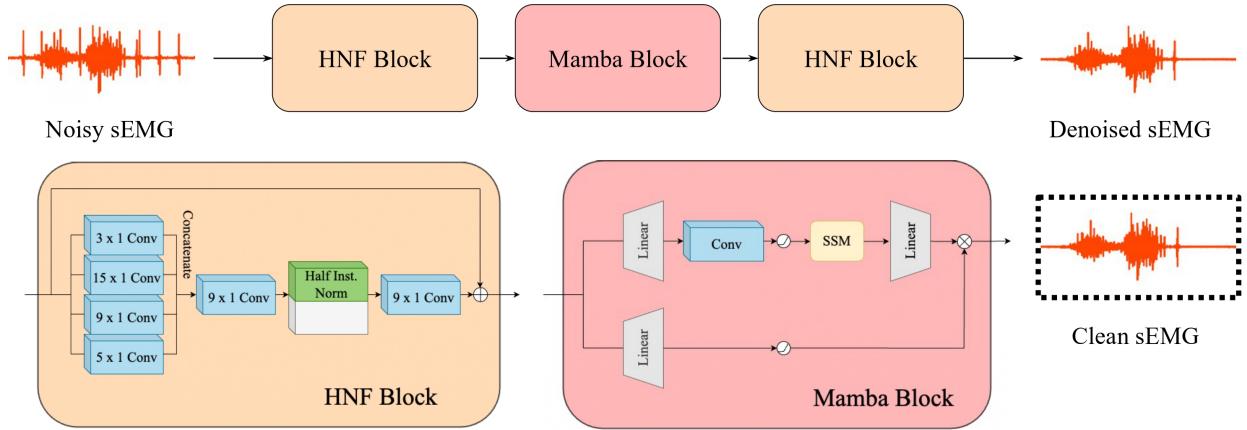


Fig. 2. The denoising framework and the model architecture of MSEM.

Recursion could be observed in equation (3, 4). Therefore, a convolution kernel  $\bar{K}$  could be introduced to relieve the computational workload.

$$\bar{K} = (C\bar{B}, C\bar{A}\bar{B}, \dots, C\bar{A}^k\bar{B}) \quad (7)$$

$$y = x * \bar{K} \quad (8)$$

One of the core concepts of the Mamba model is input awareness, i.e.,  $\bar{K}$  is constantly updated by the parameter  $\Delta$ . Hence, we could only set  $k = 0$  in Mamba. Subsequently,  $\bar{A}$ ,  $\bar{B}$ , and  $C$  is changing as well. The selective scan algorithm proposed by Gu and Dao [14] accommodates these changes efficiently.

### B. Model architecture

Fig. 2 demonstrates the denoising framework of MSEM. The key idea behind MSEM is to leverage the unique capabilities of the Mamba block to generate higher-quality outputs. The process begins with input sEMG signals being projected into the latent space through the Half Normalized Filters (HNF) Block [22], which applies various convolutional kernels to extract features at different resolutions. These features are concatenated and further processed through channel-wise convolution to match the wide frequency range of sEMG signals. Next, the Mamba block models and processes the sequence within the latent space as described in the previous subsection. Finally, the second HNF Block reconstructs the denoised sEMG signal, producing the final output. Additionally, the figure illustrates the denoising process by showing noisy, denoised, and clean sEMG. The noisy waveform represents sEMG signals under ECG interference at SNR -4 dB.

## IV. EXPERIMENTS

### A. Dataset preprocessing and preparation

The sEMG signals used in this study are sourced from the DB2 subset of the Non-Invasive Adaptive Prosthetics (NINAPro) database [23], which consists of 12-channel sEMG

recordings of hand movements from 40 subjects. These recordings were collected from the upper limb. The DB2 subset includes three sessions—Exercise 1, 2, and 3—featuring 17, 22, and 10 movements, respectively, with each movement repeated six times for five seconds, followed by a three-second rest interval. To remove potential noise in the sEMG data, a 4th-order Butterworth bandpass filter with cutoff frequencies of 20 and 500 Hz [13], [24] was applied. The signals were then downsampled to 1 kHz, normalized, and segmented into 10-second intervals.

For ECG interference, we used the MIT-BIH Normal Sinus Rhythm Database (NSRD) from PhysioNet [25], which contains 2-channel ECG recordings from 18 healthy subjects sampled at 128 Hz. Channel 1 ECG data were filtered using a 3rd-order Butterworth high-pass and low-pass filter with cutoff frequencies of 10 and 200 Hz to eliminate potential noise. Previous studies have also used this dataset for simulating ECG interference in sEMG signals [12], [13], [24].

Following prior work [13], sEMG segments from Channel 2, Exercise 1 and 3, involving 30 subjects, were used for training and validation. Each training segment had 10 randomly selected ECG signals from 12 subjects in the MIT-BIH NSRD superimposed as artifacts at six different SNR levels (-15 to -5 dB in 2 dB steps). The validation set used ECG artifacts from three other subjects with the same SNR levels. For testing, we evaluated the generalizability of the model using different subjects, movements, channels, and SNR levels. Test data were taken from Channels 9, 10, 11, and 12 in Exercise 2, involving 10 subjects. ECG signals from three remaining subjects (16420, 16539, and 16786) were used as interference, with SNR levels ranging from -14 to 0 dB in 2 dB increments.

### B. Evaluation metrics

Performance is evaluated based on the quality of signal reconstruction and feature extraction accuracy [10], [12], [13], [26]. The signal reconstruction quality is measured by the SNR improvement ( $SNR_{imp}$ ) and root-mean-square error (RMSE),

TABLE I  
OVERALL PERFORMANCE OF HP, TS, FCN, SDEMG, AND MSEMG.

|                    | $SNR_{imp}$ (dB) | RMSE            | $RMSE_{ARV}$    | $RMSE_{MF}$ (Hz) |
|--------------------|------------------|-----------------|-----------------|------------------|
| HP                 | 13.885           | 1.735e-2        | 3.064e-3        | 19.471           |
| TS                 | 14.279           | 1.626e-2        | 3.859e-3        | 23.149           |
| FCN                | 17.758           | 1.178e-2        | 3.864e-3        | 18.038           |
| SDEMG              | 18.467           | 1.138e-2        | 2.809e-3        | 14.435           |
| <b>MSEMG(Ours)</b> | <b>20.317</b>    | <b>8.603e-3</b> | <b>2.382e-3</b> | <b>11.379</b>    |

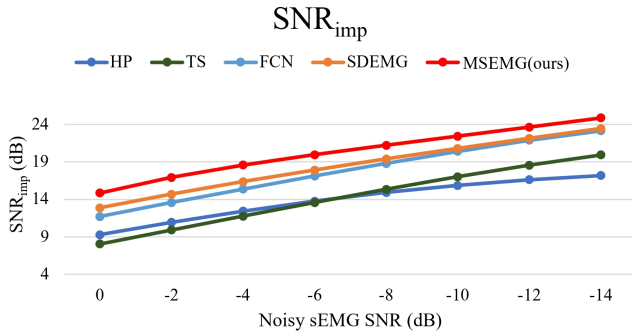


Fig. 3. Comparison of denoising methods with  $SNR_{imp}$  under various SNR conditions.

which calculate the difference between input and output SNRs and the error between output signals and the ground truth, respectively. Additionally, the RMSE of the average rectified value (ARV) and mean frequency (MF) feature vectors are used to assess sEMG feature extraction accuracy [10], [12]. These metrics are calculated following the methods in previous studies [10], [12], [13]. Higher  $SNR_{imp}$  values, lower RMSE values, and smaller RMSE values for ARV and MF indicate better signal reconstruction and higher fidelity.

### C. Results and discussion

We compare the performance of MSEMG against two traditional methods, HP and TS, and two NN-based approaches, FCN [12] and SDEMG [13]. Table I summarizes the overall results across various evaluation metrics. MSEMG consistently outperforms all other methods, achieving the highest  $SNR_{imp}$ , the lowest RMSE, and the lowest RMSE values for ARV and MF features. Fig. 3 further illustrates the  $SNR_{imp}$  performance under different SNR conditions, highlighting that MSEMG produces superior output quality across all noise interference levels. These results suggest that MSEMG offers a more robust and effective approach to sEMG denoising, largely due to its enhanced ability to capture both local and global dependencies in the data.

Fig.4 demonstrates the denoising performance in a specific scenario simulating trunk sEMG with ECG contamination. In this case, we use sEMG data from the biceps brachii (Channel 11 in NINAPro DB2) as simulation data, with the SNR set to approximately -10 dB, mimicking typical contamination con-

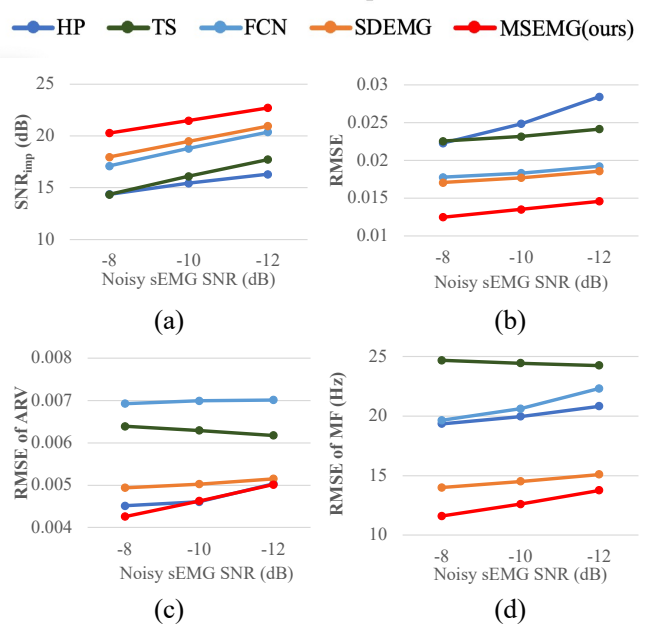


Fig. 4. Performance under the scenario simulating trunk sEMG with ECG contamination.

TABLE II  
COMPARISON OF MODEL SIZE.

|                 | FCN [12] | SDEMG [13] | <b>MSEMG(Ours)</b> |
|-----------------|----------|------------|--------------------|
| # of Parameters | 137,801  | 1,233,857  | 279,937            |

ditions in trunk sEMG [10], [11], [27]. Under these conditions, MSEMG can still maintain its superiority across all evaluation metrics.

Table II compares the number of trainable parameters in the NN-based denoising models. MSEMG is about one-fifth the size of SDEMG, the previous state-of-the-art method. Given MSEMG's superior performance in removing ECG artifacts and its smaller model size, we conclude that MSEMG offers an efficient and effective solution for sEMG denoising.

### V. CONCLUSION

In this study, we present MSEMG, a novel denoising model that combines the Mamba state space model with CNNs. MSEMG effectively captures both local and global dependencies in sEMG signals while maintaining low computational costs. Our experimental results demonstrate that MSEMG consistently outperforms previous methods across all evaluation metrics, even under varying SNR conditions. These findings highlight MSEMG as a promising solution for sEMG denoising in a wide range of applications. Future work will focus on further optimizing MSEMG's performance with additional data and more complex denoising scenarios. We also plan to apply MSEMG to downstream tasks such as hand gesture recognition and respiratory estimation to assess its effectiveness in real-world applications.

## REFERENCES

- [1] X. Tang, X. Zhang, X. Gao, et al., "A novel interpretation of sample entropy in surface electromyographic examination of complex neuromuscular alternations in subacute and chronic stroke," *IEEE Transactions on Neural Systems and Rehabilitation Engineering*, vol. 26, no. 9, pp. 1878–1888, 2018.
- [2] S. M. Engdahl, B. P. Christie, et al., "Surveying the interest of individuals with upper limb loss in novel prosthetic control techniques," *Journal of neuroengineering and rehabilitation*, vol. 12, no. 1, pp. 1–11, 2015.
- [3] J. Wijsman, B. Grundlehner, H. Liu, et al., "Wearable physiological sensors reflect mental stress state in office-like situations," in *Proc. ACII*, 2013.
- [4] N. J. Domnik, E. S. Walsted, and D. Langer, "Clinical utility of measuring inspiratory neural drive during cardiopulmonary exercise testing (cpet)," *Frontiers in Medicine*, vol. 7, pp. 483, 2020.
- [5] N. L. Vandebussche, S. Overeem, J. P. van Dijk, P. J. Simons, and D. A. Pevernagie, "Assessment of respiratory effort during sleep: esophageal pressure versus noninvasive monitoring techniques," *Sleep medicine reviews*, vol. 24, pp. 28–36, 2015.
- [6] J. Ma, N. V. Thakor, and F. Matsuno, "Hand and wrist movement control of myoelectric prosthesis based on synergy," *IEEE Transactions on Human-Machine Systems*, vol. 45, no. 1, pp. 74–83, 2014.
- [7] U. Cote-Allard, G. Gagnon-Turcotte, A. Phinyomark, K. Glette, E. Scheme, F. Laviolette, and B. Gosselin, "A transferable adaptive domain adversarial neural network for virtual reality augmented emg-based gesture recognition," *IEEE Transactions on Neural Systems and Rehabilitation Engineering*, vol. 29, pp. 546–555, 2021.
- [8] Y. Xiao, H. Bai, Y. Gao, B. Hu, J. Zheng, X. Cai, J. Rao, X. Li, and A. Hao, "Interactive virtual ankle movement controlled by wrist semg improves motor imagery: An exploratory study," *IEEE Transactions on Visualization and Computer Graphics*, 2023.
- [9] D. A. Winter, *Biomechanics and motor control of human movement*, John Wiley & Sons, 2009.
- [10] L. Xu, E. Peri, R. Vullings, et al., "Comparative review of the algorithms for removal of electrocardiographic interference from trunk electromyography," *Sensors*, vol. 20, no. 17, pp. 4890, 2020.
- [11] J. D. Drake and J. P. Callaghan, "Elimination of electrocardiogram contamination from electromyogram signals: An evaluation of currently used removal techniques," *Journal of electromyography and kinesiology*, vol. 16, no. 2, pp. 175–187, 2006.
- [12] K.-C. Wang, K.-C. Liu, S.-Y. Peng, and Y. Tsao, "Ecg artifact removal from single-channel surface emg using fully convolutional networks," in *Proc. ICASSP*, 2023.
- [13] Y.-T. Liu, K.-C. Wang, K.-C. Liu, S.-Y. Peng, and Y. Tsao, "Sdemg: Score-based diffusion model for surface electromyographic signal denoising," in *Proc. ICASSP*, 2024.
- [14] A. Gu and T. Dao, "Mamba: Linear-time sequence modeling with selective state spaces," *arXiv preprint arXiv:2312.00752*, 2023.
- [15] A. Vaswani, "Attention is all you need," *Advances in Neural Information Processing Systems*, 2017.
- [16] O. Lieber, B. Lenz, H. Bata, G. Cohen, J. Osin, I. Dalmedigos, E. Safahi, S. Meiroum, Y. Belinkov, S. Shalev-Shwartz, et al., "Jamba: A hybrid transformer-mamba language model," *arXiv preprint arXiv:2403.19887*, 2024.
- [17] R. Chao, W.-H. Cheng, M. La Quatra, S. M. Siniscalchi, C.-H. H. Yang, S.-W. Fu, and Y. Tsao, "An investigation of incorporating mamba for speech enhancement," *arXiv preprint arXiv:2405.06573*, 2024.
- [18] J. D. C. Junior, J. M. de Seixas, et al., "A template subtraction method for reducing electrocardiographic artifacts in emg signals of low intensity," *Biomedical Signal Processing and Control*, vol. 47, pp. 380–386, 2019.
- [19] S. Shams, S. S. Dindar, X. Jiang, and N. Mesgarani, "Ssamba: Self-supervised audio representation learning with mamba state space model," *arXiv preprint arXiv:2405.11831*, 2024.
- [20] J. Zhang, C. Song, T. Cui, C. Li, and J. Ma, "ChiMamba: Predicting Chromatin Interactions Based on Mamba," in *Proc. ICIC*, 2024.
- [21] V. Thoutam and D. Ellsworth, "MSAMamba: Adapting Subquadratic Sequence Models to Long-Context DNA MSA Analysis," in *Proc. ICIST*, 2024.
- [22] F. P. Romero, D. C. Piñol, and C. R. Vázquez-Seisdedos, "Deepfilter: An ecg baseline wander removal filter using deep learning techniques," *Biomedical Signal Processing and Control*, vol. 70, pp. 102992, 2021.
- [23] M. Atzori, A. Gijsberts, C. Castellini, et al., "Electromyography data for non-invasive naturally-controlled robotic hand prostheses," *Scientific data*, vol. 1, no. 1, pp. 1–13, 2014.
- [24] J. Machado, A. Machado, and A. Balbinot, "Deep learning for surface electromyography artifact contamination type detection," *Biomedical Signal Processing and Control*, vol. 68, pp. 102752, 2021.
- [25] A. L. Goldberger, L. A. Amaral, L. Glass, et al., "Physiobank, physiobank, and physionet: components of a new research resource for complex physiologic signals," *circulation*, vol. 101, no. 23, pp. e215–e220, 2000.
- [26] H.-T. Chiang, Y.-Y. Hsieh, S.-W. Fu, et al., "Noise reduction in ecg signals using fully convolutional denoising autoencoders," *Ieee Access*, vol. 7, pp. 60806–60813, 2019.
- [27] P. Zhou and T. A. Kuiken, "Eliminating cardiac contamination from myoelectric control signals developed by targeted muscle reinnervation," *Physiological Measurement*, vol. 27, no. 12, pp. 1311, 2006.